JCI The Journal of Clinical Investigation

Circular RNA cia-MAF drives self-renewal and metastasis of liver tumor-initiating cells via transcription factor MAFF

Zhenzhen Chen, … , Zusen Fan, Pingping Zhu

J Clin Invest. 2021;131(19):e148020. https://doi.org/10.1172/JCI148020.

Research Article | Cell biology | Oncology

Graphical abstract

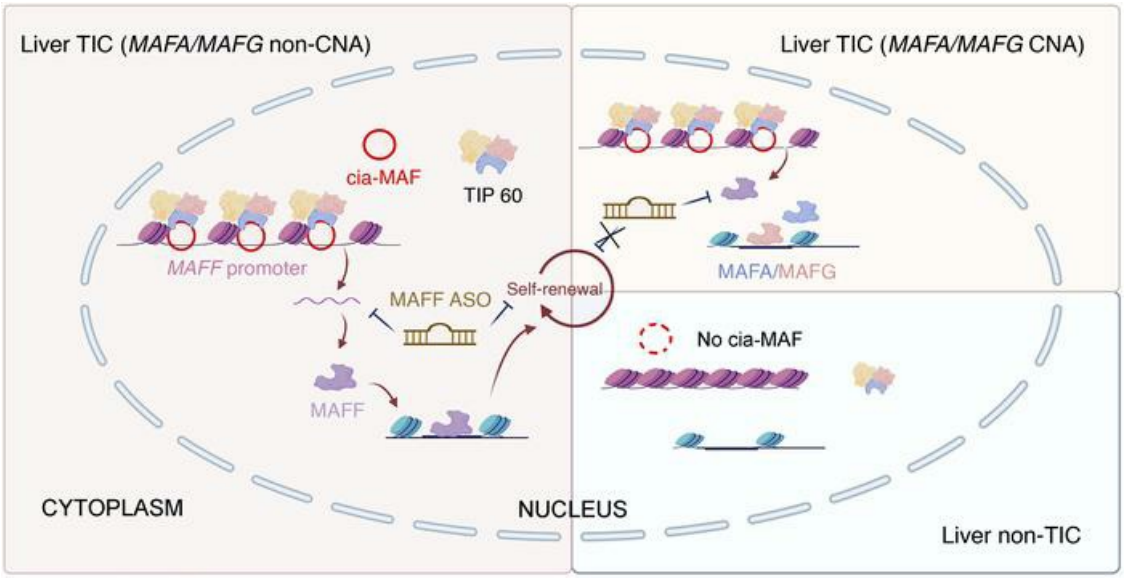

Circular RNA cia-MAF drives self-renewal and metastasis of liver tumor-initiating cells via transcription factor MAFF

Zhenzhen Chen,[1] Tiankun Lu,[2,3] Lan Huang,[4] Zhiwei Wang,[1] Zhongyi Yan,[5] Yubo Guan,[1] Wenjing Hu,[1] Zusen Fan,[2,3] and Pingping Zhu[1,6]

[1]School of Life Sciences, Zhengzhou University, Zhengzhou, China. [2]University of Chinese Academy of Sciences, Beijing, China. [3]CAS Key Laboratory of Infection and Immunity, CAS Center for Excellence in Biomacromolecules, Institute of Biophysics, Chinese Academy of Sciences, Beijing, China. [4]Biotherapy Center, The First Affiliated Hospital of Zhengzhou University, Zhengzhou, Henan, China. [5]School of Basic Medical Sciences, Henan University, Kaifeng, China. [6]State Key Laboratory of Esophageal Cancer Prevention & Treatment, Zhengzhou University, Zhengzhou, Henan Province, China.

Liver tumor-initiating cells (TICs) are involved in liver tumorigenesis, metastasis, drug resistance, and relapse, but the regulatory mechanisms of liver TICs are largely unknown. Here, we have identified a functional circular RNA, termed circRNA activating MAFF (cia-MAF), that is robustly expressed in liver cancer and liver TICs. *cia-MAF*–KO primary cells and *cia-maf*–KO liver tumors harbor decreased ratios of TICs, and display impaired liver tumorigenesis, self-renewal, and metastatic capacities. In contrast, cia-MAF overexpression drives liver TIC propagation, self-renewal, and metastasis. Mechanistically, cia-MAF binds to the *MAFF* promoter, recruits the TIP60 complex to the *MAFF* promoter, and finally promotes MAFF expression. Loss of cia-MAF function attenuates the combination between the TIP60 complex and the *MAFF* promoter. MAFF is highly expressed in liver tumors and liver TICs, and its antisense oligo (ASO) has therapeutic potential in treating liver cancer without *MAFA*/*MAFG* gene copy number alterations (CNAs). This study reveals an additional layer for liver TIC regulation as well as circRNA function, and provides an additional target for eliminating liver TICs, especially for liver tumors without *MAFA*/*MAFG* gene CNAs.

Introduction

Liver cancer, the incidence of which is continuously increasing, is the third leading cause of cancer-related deaths. About 90% liver cancers are hepatocellular carcinoma (HCC) (1). Despite surgical resection, radiotherapy, chemotherapy, and liver transplantation, the prognosis of patients with HCC is very poor, mainly because of the significant heterogeneity of HCC (2). Recent studies have shown that tumor heterogeneity is due to the hierarchical organization of tumor cells within the tumor bulk, which is generated from a small subset of cells, termed tumor-initiating cells (TICs) or cancer stem cells (CSCs) (2). Unlike non-TICs, TICs harbor the ability to self-renew, differentiate, and generate new tumors. Moreover, TICs are resistant to conventional therapies, including radiotherapy and chemotherapy (3). Accumulating studies demonstrate that TICs are also resistant to immunotherapy, including chimeric antigen receptor (CAR) T cell and immune checkpoint therapies (4, 5). Several liver TIC markers have been identified, including CD44, CD13, CD133, and EPCAM (6). Some up to date technologies, including single-cell RNA sequencing and CRISPR-Cas9–based genome editing, have facilitated the characterization and functional investigation of TICs (7, 8). However, the mechanisms involved in liver TIC self-renewal remain elusive.

Like normal stem cells, TICs rely on stemness signaling pathways to maintain their self-renewal and differentiation capacities, and these pathways are precisely regulated. Accumulating evidence demonstrates that the alterations in stemness pathways, including Wnt/β-catenin, Notch, and Hedgehog pathways, lead to tumorigenesis and tumor progression (9). On the one hand, hyperactivation of these pathways in normal stem cells leads to their expansion and abnormal differentiation, resulting in tissue-specific tumorigenesis. On the other hand, abnormal activation of these pathways in differentiated tumor cells triggers their dedifferentiation process (10). Thus, these pathways need to be precisely regulated by multiple modulators, including transcription factors, chromatin remodeling factors, and regulatory RNAs (11). Recently, several niche factors have been identified as TIC regulators (12, 13). We previously identified several long noncoding RNAs that regulate the self-renewal of liver TICs via the Wnt/β-catenin, Hedgehog, and Hippo/Yap1 pathways, in intracellular or niche-dependent manners (14–16).

Transcription factors (TFs) are sequence-specific DNA-binding factors and play central roles in cell fate determination. TFs bind to the promoter region of target genes to promote or inhibit their expression. The MAF family of TFs are basic leucine zipper TFs, which contain a highly conserved homology region and a basic region. The MAF TFs regulate gene expression and differentiation in a wide variety of tissues and are also involved in human diseases, including tumorigenesis (17, 18). There are 5 MAF TFs in human cells: MAFA, MAFB, MAFF, MAFG, and MAFK. Recent studies have revealed that MAFF promotes tumor invasion and metastasis as a hypoxia gene, but its role in liver TICs remains unknown (19). In this study, we revealed that MAFF is required for

Authorship note: ZC and TL contributed equally to this work.
Conflict of interest: The authors have declared that no conflict of interest exists.

Submitted: January 25, 2021; **Accepted:** August 12, 2021; **Published:** October 1, 2021.
Reference information: *J Clin Invest*. 2021;131(19):e148020.
https://doi.org/10.1172/JCI148020.

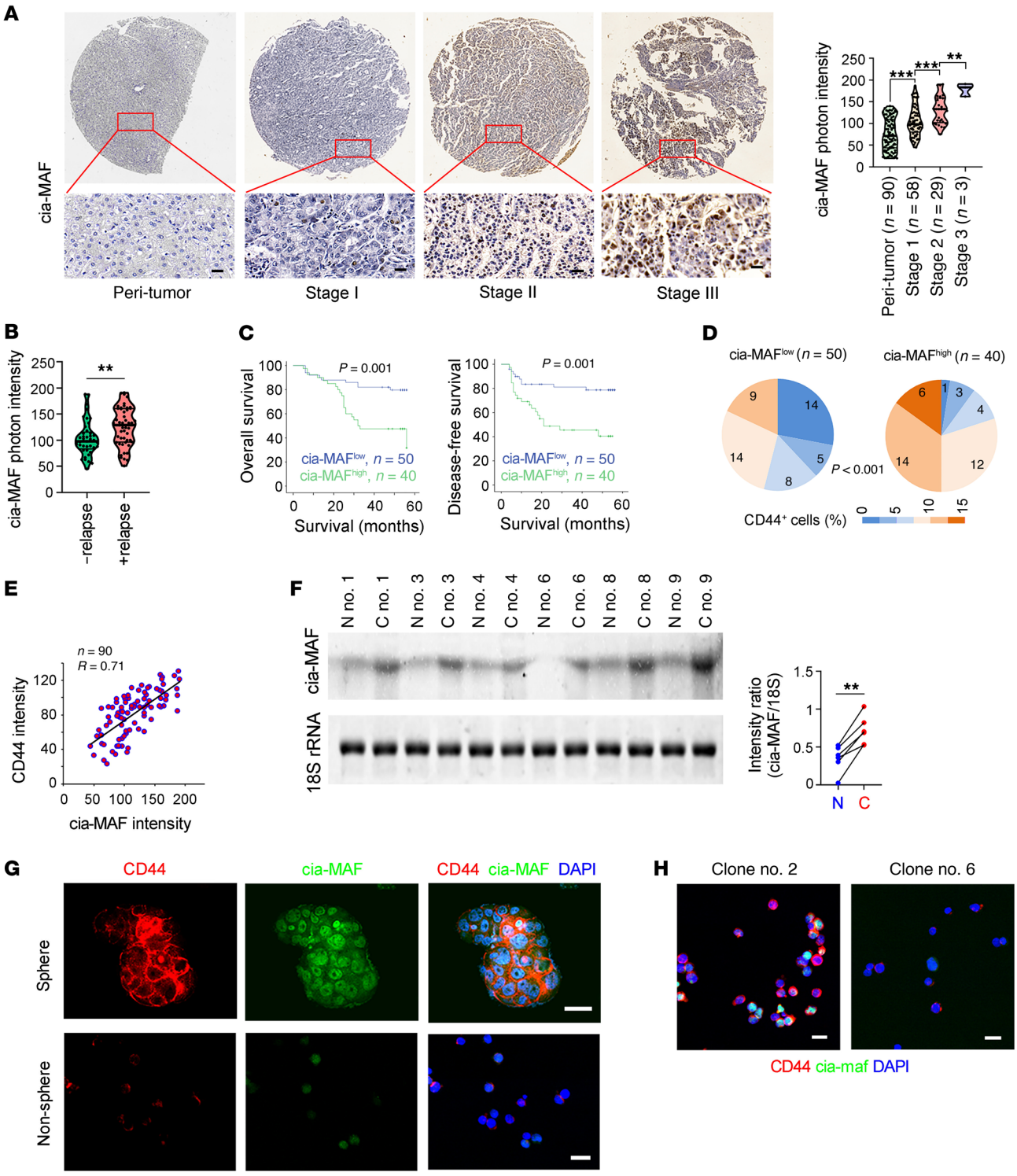

Figure 1. cia-MAF is highly expressed in liver cancer and TICs. (**A**) In situ hybridization of cia-MAF in HCC tissue microarray containing 90 peri-tumor, 58 stage 1, 29 stage 2, and 3 stage 3 tumor tissues. Typical images are in the left panels and calculated intensities are in the right panel. Scale bars: 30 μm. The details of HCC tissue microarray are listed in Supplemental Table 4. (**B**) Violin plot showing cia-MAF intensities in HCC samples with (+) or without (–) relapse. Individual samples, medium levels, minimum, maximum, and quarter levels are shown. (**C**) Kaplan–Meier survival analysis of cia-MAF^{hi} and cia-MAF^{lo} samples, which are grouped according to the average cia-MAF expression level. (**D**) Percentage distribution of CD44$^+$ TICs in cia-MAF^{lo} (left) and cia-MAF^{hi} (right) samples. (**E**) Coexpression of cia-MAF and liver TIC marker CD44 in 90 liver cancer tissues. (**F**) Northern blot of cia-MAF in CD44$^+$ TICs (**C**) and CD44$^-$ non-TICs (N). 18S rRNA served as a loading control. Typical images are in the left panel and signal intensities are quantified with Image J (right). (**G**) FISH of cia-MAF in spheres and nonspheres, which were derived from primary HCC cells. Scale bars: 20 μm. (**H**) FISH of cia-Maf in clone #2 and clone #6, which were derived from YFP$^+$ mouse liver cancer cells. Scale bars: 20 μm. $^*P < 0.05$, $^{**}P < 0.05$, $^{***}P < 0.001$. Significance was determined by 1-tailed Student's *t* test (**A**, **B**, and **F**), log-rank test (**C**), and χ^2 test (**D**). For all representative images, *n* = 3 independent experiments performed with similar results.

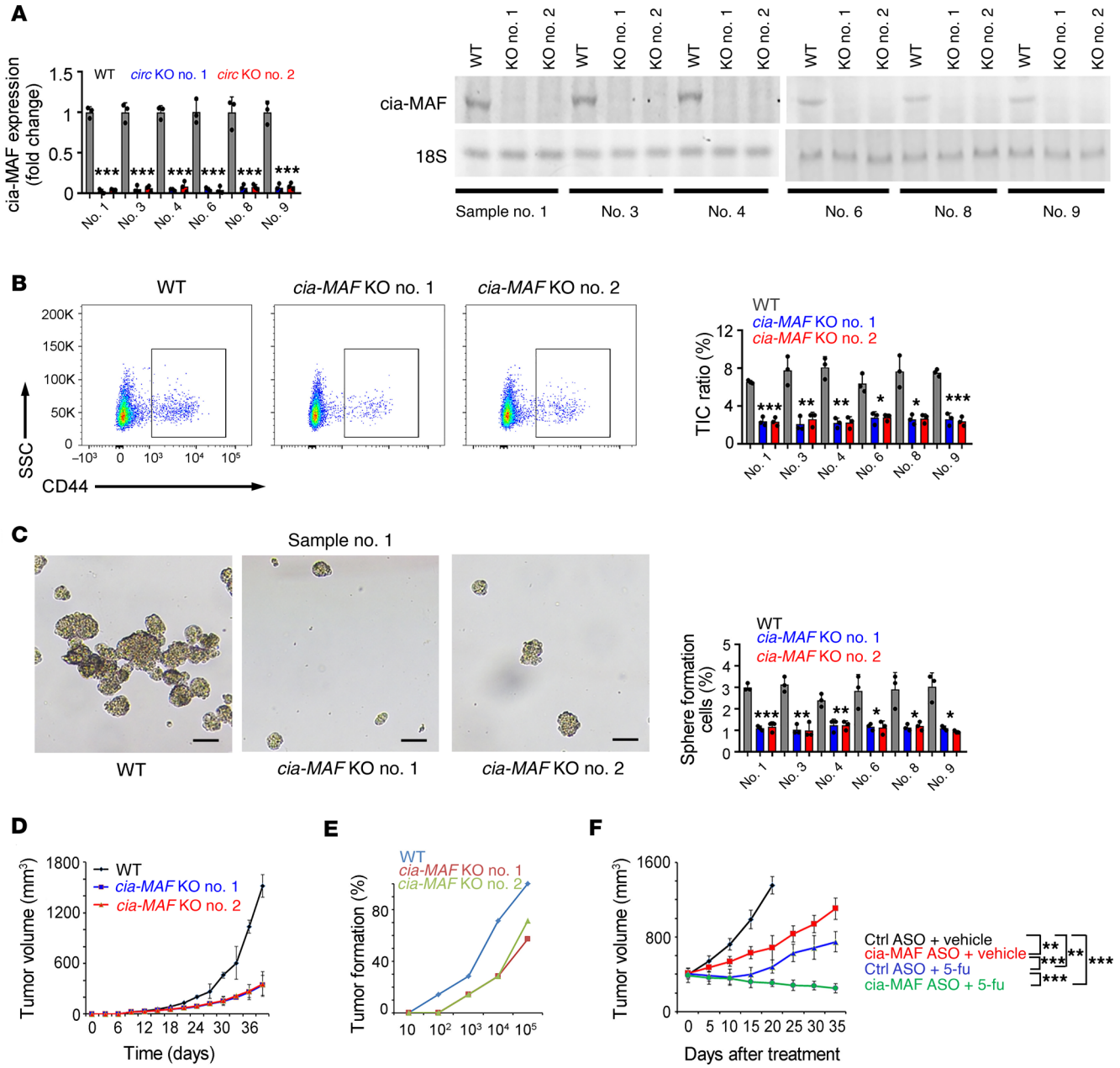

Figure 2. *cia-MAF* knock out impairs liver TIC self-renewal. (**A**) Real-time PCR (left) and Northern blot (right) analyses for *cia-MAF* knockout efficiency. circ KO, *cia-MAF* knock out. (**B**) CD44 FACS for TIC detection, using *cia-MAF*–KO and control cells. $n = 3$ independent samples for detection. (**C**) Sphere formation of *cia-MAF*–KO cells, with typical images in the left panels and sphere formation ratios in the right panel. Scale bars: 500 μm. (**D**) Tumor propagation of WT and *cia-MAF*–KO cells, which were subcutaneously injected into BALB/c nude mice. Tumor volumes were measured every 3 days. (**E**) Three months of tumor initiation assay using gradient numbers of *cia-MAF*–KO and control cells. $n = 7$ mice for each group and the ratios of tumor formation mice are shown. (**F**) Propagation of patient-derived xenografts after the indicated treatments, which were performed when xenograft volume reach about 400 mm^3. In all panels, data are shown as mean ± SD. $^*P < 0.05$, $^{**}P < 0.01$, and $^{***}P < 0.001$ by 1-way ANOVA. For all representative images, n=3 independent experiments performed with similar results.

liver TIC self-renewal and that MAFF antisense oligo (ASO) has therapeutic effects on liver cancer without *MAFA*/*MAFG* gene copy number alterations (CNAs).

Circular RNAs (circRNAs), formed by covalent conjugation of 5′ and 3′ ends through backsplicing, recently emerged as critical modulators in various biological processes (20). circRNAs are generated from their parent pre-mRNAs, and grouped into extron circRNAs, intron circRNAs, and extron-intron circRNAs (21). Recent studies revealed the key roles of circRNAs in many physiological and pathological processes, including neuropsychiatric disorders, tumorigenesis, and immunological regulation (22–24). Several circRNAs, including ciRS-7/CDR1as, circHIPK3, and Sry circRNA, act as microRNA (miRNA) sponges (25, 26). Interestingly, fusion circRNA derived from cancer-associated chromosomal translocations are involved in tumorigenesis and therapy resistance (27). We previously identified circPan3 and circKcnt2 as regulators of intestinal stem cell self-renew-

al and colitis progression (28, 29). However, it is unclear whether and how circRNAs regulate liver TIC self-renewal. In this study, we identified that a circRNA termed circRNA activating MAFF (cia-MAF) was highly expressed in liver cancer and liver TICs, and we evaluated its biological roles using primary samples and *cia-maf*–KO mice. We found that cia-MAF binds to the *MAFF* promoter and recruits TIP60 complex, a chromatin remodeling complex required for MAFF transcription, and ultimately drives the self-renewal of liver TICs.

Results

High expression of cia-MAF in liver cancer and TICs. Liver TICs drive liver tumorigenesis, metastasis, and drug resistance, and their self-renewal needs to be precisely regulated. To identify functional circRNAs in liver TICs, we reanalyzed our circRNA data set (GSE78520), and selected the top 10 circRNAs with the highest expression in TICs (Supplemental Figure 1A; supplemental material available online with this article; https://doi.org/10.1172/JCI148020DS1). These transcripts were resistant to RNase R and actinomycin D treatment, confirming that they are circRNAs (Supplemental Figure 1B). Among these 10 circRNAs, we focused on cia-MAF as a functional circRNA involved in liver TIC self-renewal (Supplemental Figure 1, C and D). Moreover, cia-MAF was highly conserved among various species (Supplemental Table 1).

cia-MAF was highly expressed in liver cancer, and its expression levels were correlated with the clinical severity (Figure 1A), as well as tumor relapse (Figure 1B), patient prognosis (Figure 1C), and the expression of TIC marker CD44 (Figure 1, D and E). Another tissue microarray also confirmed that cia-MAF was highly expressed in liver cancer and its expression was related to clinical prognosis (Supplemental Figure 2, A and B, and Supplemental Table 5). We then examined the expression landscape of cia-MAF in liver TICs, and found that it was highly expressed in liver TICs and spheres (Figure 1, F and G, and Supplemental Figure 2, C–E). These data confirm that cia-MAF is highly expressed in liver cancer and liver TICs.

In mice, the expression levels of cia-MAF homologous transcript (hereafter termed as cia-maf) were increased along with DEN/CCl4-induced tumorigenesis (Supplemental Figure 2, F and G). Forty-eight clones derived from single tumor cells had divergent expression levels of cia-maf and CD44, and $CD44^{hi}$ clones showed increased cia-maf expression (Supplemental Figure 2, H and I). The robust expression of cia-maf in $CD44^{hi}$ clones was confirmed by FISH (Figure 1H). Then sphere formation assay was performed and 5 sphere clones were derived from single cells, and cia-maf expression was increased in spheres (Supplemental Figure 2, J and K). Overall, these results demonstrate that cia-MAF is robustly expressed in liver TICs enriched from primary samples and DEN/CCl4-induced mouse tumors.

cia-MAF promotes liver TIC self-renewal. To explore the role of cia-MAF in liver TIC self-renewal, we generated *cia-MAF*–KO cells using a CRISPR/Cas9 approach (Supplemental Figure 3, A–C). *cia-MAF* knock out remarkably abolished cia-MAF expression but not linear mRNA expression (Figure 2A and Supplemental Figure 3, D and E). The *cia-MAF*–KO cells harbored fewer TICs (Figure 2B and Supplemental Figure 3F). Moreover, sphere formation and tumor invasion capacities were attenuated in *cia-MAF*–KO cells (Figure 2C and Supplemental Figure 3G). *cia-MAF* knock out also inhibited tumor propagation and tumor-initiating capacities (Figure 2, D and E, and Supplemental Table 2A). Interestingly, *cia-MAF* knock out moderately inhibited the propagation and transwell capacities of non-TICs, probably because of the low expression of cia-MAF in non-TICs (Supplemental Figure 3, H–J). Moreover, cia-MAF antisense oligo (ASO) enhanced the anti-tumor efficiency of 5-fluorouracil by eliminating TICs (Figure 2F). These data demonstrate the essential role of cia-MAF in human liver TIC self-renewal.

We then evaluated the role of cia-maf in mouse liver TICs. In clones with high cia-maf expression, cia-maf knock down inhibited tumor initiation (Supplemental Figure 4, A and B) and sphere formation (Supplemental Figure 4, C and D). These data reveal the critical roles of cia-maf in mouse liver TIC self-renewal. Then *cia-maf*–KO mice were generated using a CRISPR/Cas9 approach (Supplemental Figure 4, E–H). *cia-maf*–KO mice showed no *cia-maf* expression but the expression of linear mRNA was comparable to their littermate WT mice (Supplemental Figure 4, I–L). DEN/CCl4-induced liver tumorigenesis was reduced in *cia-maf*–KO mice, with decreased numbers of liver progenitor cells, proliferating cells, and TICs, whereas apoptotic cells, $F4/80^{+}$ cells, and fibrosis were comparable between *cia-maf*–KO and control mice (Figure 3, A–D, and Supplemental Figure 4, M–O). Moreover, *cia-maf*–KO TICs exhibited impaired sphere formation capacity, and CD44 expression was decreased in these spheres (Figure 3, E and F). Interestingly, cia-maf was also required for liver tumorigenesis in a HrasG12V plus shp53 hydrodynamic injection model (Figure 3G and Supplemental Figure 4P).Taking advantage of tumor transplantation, we proved that cia-maf is an intrinsic factor in the regulation of liver tumor propagation (Supplemental Figure 4Q).

Next, we established cia-MAF–overexpressing cells, which contained increased ratios of liver TICs (Figure 4, A and B). cia-MAF overexpression enhanced the sphere formation (Figure 4C), tumor invasion (Figure 4D), and tumor initiation capacities (Figure 4E and Supplemental Table 2B). cia-maf overexpression rescued the self-renewal and tumor initiation capacities of liver tumor cells with low cia-maf expression (Figure 4, F–H). Overall, these results confirm that cia-MAF promotes the self-renewal of liver TICs.

cia-MAF drives TIC self-renewal by targeting MAFF. To explore the molecular mechanism of cia-maf in liver TIC regulation, we performed RNA sequencing using *cia-maf*–KO TICs and validated the RNA-seq data with real-time PCR (Supplemental Figure 5A). Transcription-associated genes were enriched among the differently expressed genes in *cia-maf*–KO TICs, thus we focused on the function of cia-maf in transcriptional regulation (Supplemental Figure 5B). Among the top 10 downregulated transcription factors in *cia-maf*–KO cells, MAFF showed the most important role in sphere formation (Figure 5, A and B, and Supplemental Figure 5, C and D). Of note, MAFF and cia-MAF were coexpressed in clinical HCC samples (Supplemental Figure 5E). These data indicated that MAFF served as a functional target gene of cia-MAF in liver TIC self-renewal. Therefore, we generated *MAFF*-KO cells using a CRISPR/Cas9 approach (Figure 5C). These cells contained a decreased ratio of liver TICs, and displayed impaired self-renewal and invasion capacities (Figure 5, D and E, and Supplemental Figure 5F). Interestingly, MAFF bound to *CD44* promoter (Supplemental Figure 5G), and CD44 expression levels were decreased in *cia-MAF*–KO and *MAFF*-KO cells (Supplemental Figure 5H). These data demonstrate that cia-MAF targets MAFF, which is required for liver TIC self-renewal and CD44 expression.

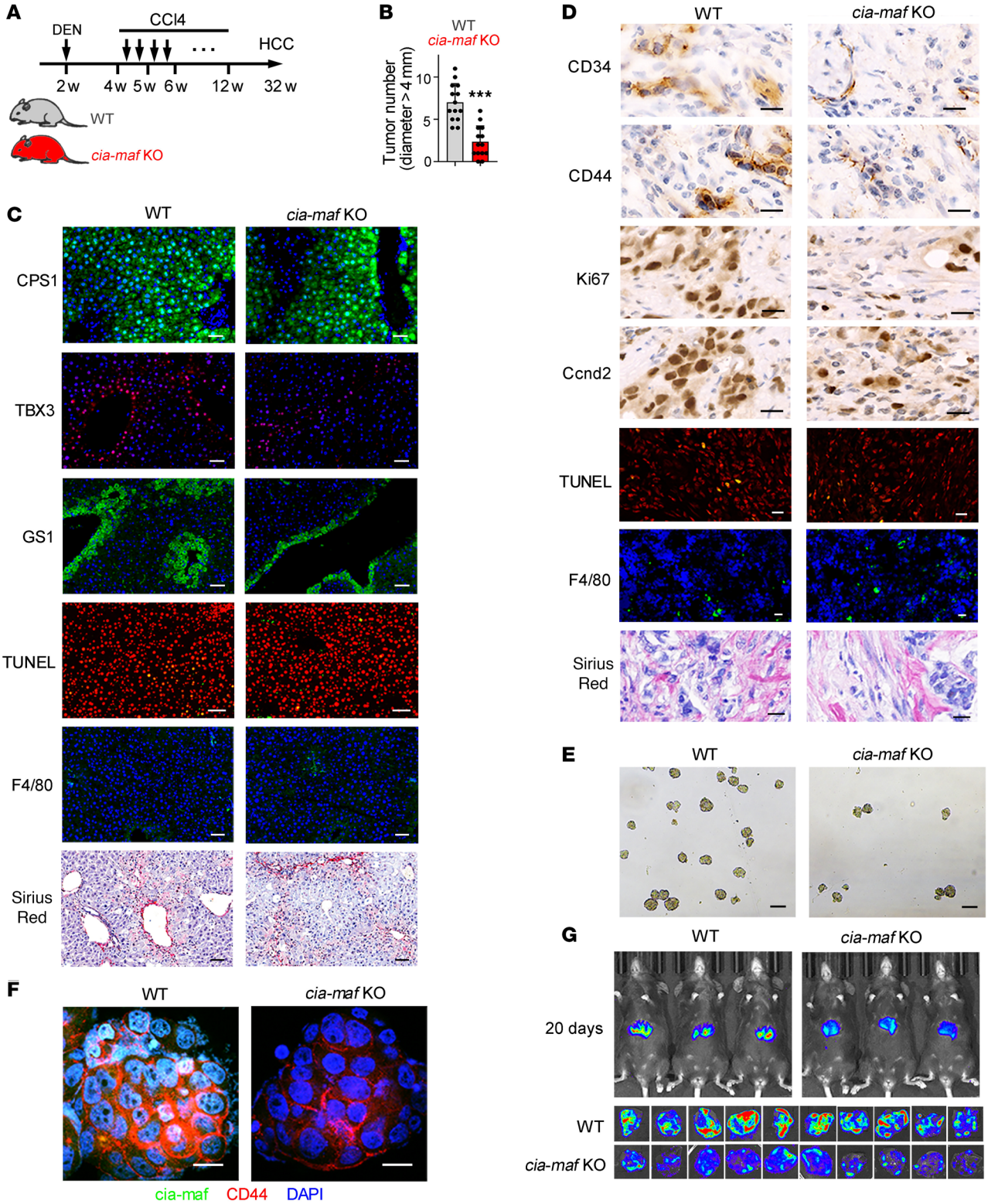

Figure 3. *cia-maf*–KO mice harbor impaired liver tumorigenesis and self-renewal capacities. (**A**) Schematic diagram of DEN/CCl4 liver tumorigenesis. WT and *cia-maf* KO mice were used. (**B**) Tumor numbers of WT and *cia-maf* KO mice at 32 weeks. $n = 14$ mice were detected for each group. Data are shown as mean ± SD. $^{**}P < 0.01$, by 1-tailed Student's t test. (**C**) Typical images of CPS1, TBX3, GS1, TUNEL, F4/80, and Sirius Red staining in WT and *cia-maf*–KO peri-tumor liver tissues, which were performed using DEN/CCl4-induced livers. Scale bars: 50 μm. (**D**) Typical images of CD34, CD44, Ki67, Ccnd2, TUNEL, F4/80, and Sirius Red staining in WT and *cia-maf*–KO tumors. All samples were derived from DEN/CCl4-treated mice. Scale bars: 20 μm. (**E**) Sphere formation assay of WT and *cia-maf*–KO TICs, which was sorted from WT and *cia-maf*–KO tumors. Scale bars: 500 μm. (**F**) FISH for cia-maf expression and immunofluorescence for CD44 expression in WT and *cia-maf*–KO spheres. Scale bars: 10 μm. (**G**) HrasG12V and shP53 plasmid, along with luciferase and SB transposase plasmid, were injected into *cia-maf*–KO and littermate mice, and tumor propagation was measured via luciferase signals. For **C** and **D**, $n = 10$ images taken with similar results. For **E** and **F**, $n = 3$ independent experiments performed with similar results. For **G**, $n = 10$ mice per group.

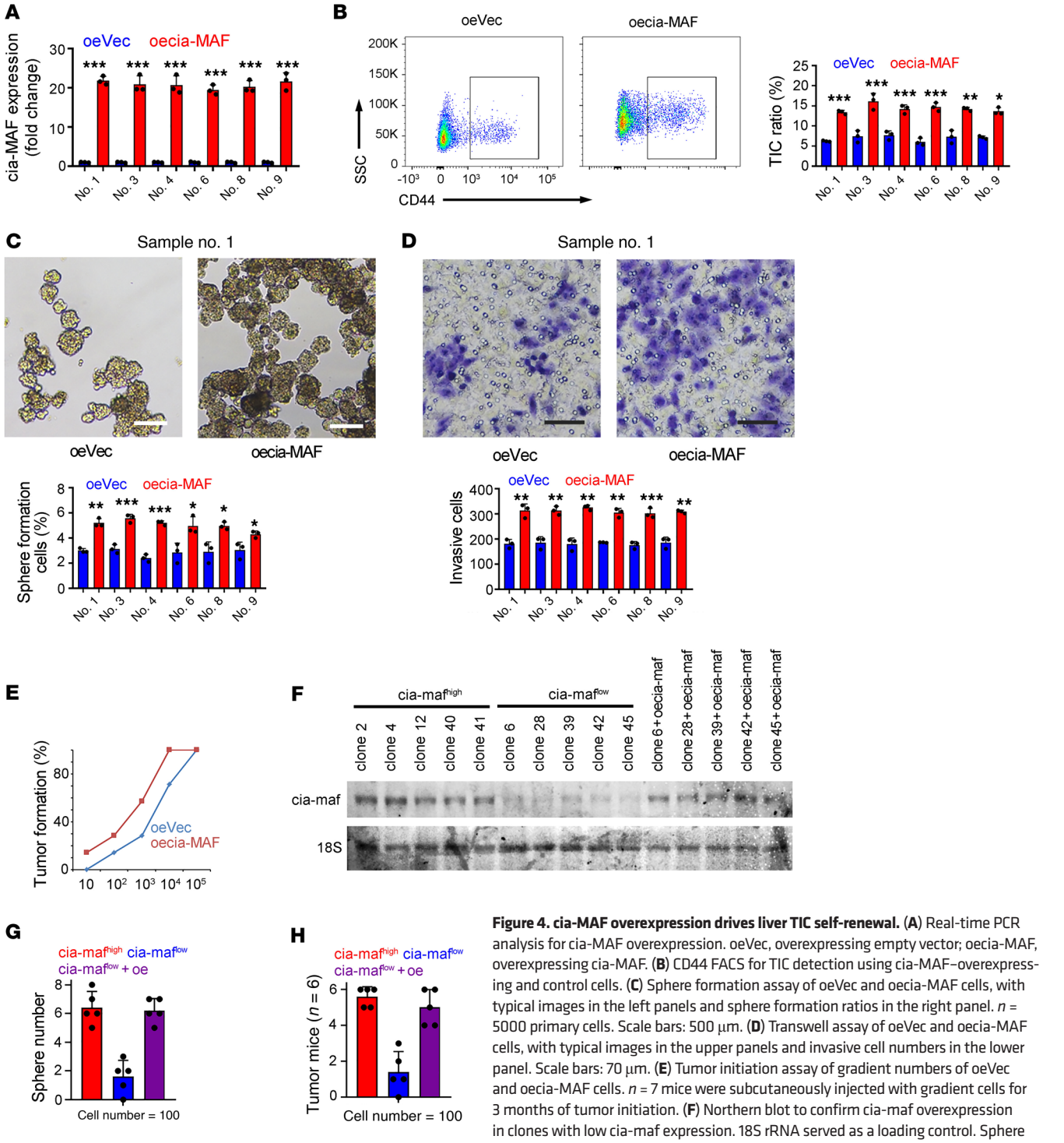

Figure 4. cia-MAF overexpression drives liver TIC self-renewal. (**A**) Real-time PCR analysis for cia-MAF overexpression. oeVec, overexpressing empty vector; oecia-MAF, overexpressing cia-MAF. (**B**) CD44 FACS for TIC detection using cia-MAF–overexpressing and control cells. (**C**) Sphere formation assay of oeVec and oecia-MAF cells, with typical images in the left panels and sphere formation ratios in the right panel. n = 5000 primary cells. Scale bars: 500 μm. (**D**) Transwell assay of oeVec and oecia-MAF cells, with typical images in the upper panels and invasive cell numbers in the lower panel. Scale bars: 70 μm. (**E**) Tumor initiation assay of gradient numbers of oeVec and oecia-MAF cells. n = 7 mice were subcutaneously injected with gradient cells for 3 months of tumor initiation. (**F**) Northern blot to confirm cia-maf overexpression in clones with low cia-maf expression. 18S rRNA served as a loading control. Sphere formation (**G**) and tumor initiation (**H**) capacities of cia-maf^{hi} clones, cia-maf^{lo} clones, and cia-maf–overexpressing clones. One hundred single cells were used for each clone. In all panels, data are shown as mean ± SD. $^*P < 0.05$, $^{**}P < 0.01$, and $^{***}P < 0.001$ by 1-tailed Student's t test. For **A**–**F**, n = 3 independent experiments performed with similar results. For **G** and **H**, n = 5 clones examined for each group.

To explore the role of MAFF in cia-MAF function, cia-MAF was silenced or overexpressed in *MAFF*-KO cells. The effects of cia-MAF in liver TIC self-renewal and metastasis were abolished in *MAFF*-KO cells, highlighting the essential role of MAFF in cia-MAF function (Supplemental Figure 6, A and B). Rescue of MAFF expression in *cia-MAF*–KO cells restored their self-renewal and metastatic capacities, whereas rescue of CD44 expression partially restored TIC functions, indicating that cia-MAF mainly exerted its role through MAFF, and cia-MAF/MAFF worked via CD44-dependent and CD44-independent manners (Supplemental Fig-

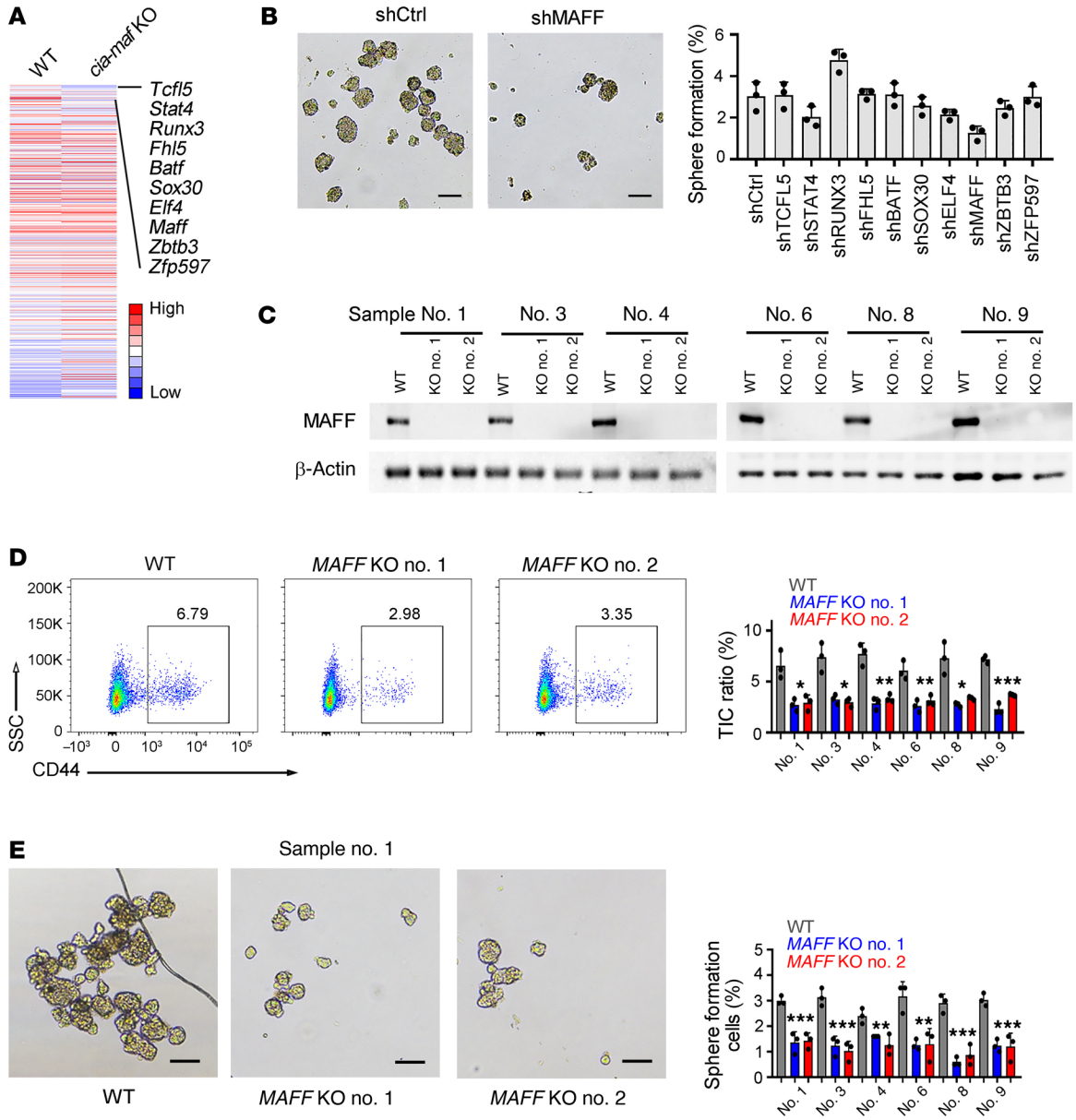

Figure 5. cia-MAF targets MAFF to initiate TIC self-renewal. (**A**) Heatmap of TF expression levels in WT and *cia-maf*–KO liver TICs. The top 10 TFs with decreased expression in *cia-maf*–KO liver TICs are listed in the right panel. For WT and *cia-maf*–KO liver TICs, liver TICs from 5 mice were pooled together for RNA-seq. WT littermates were used as controls. (**B**) Sphere formation of primary cells in which the indicated TFs were silenced individually. Scale bars: 500 μm. (**C**) Western blot to detect knockout efficiency using *MAFF*-KO and control cells. β-actin was a loading control. (**D**) CD44 FACS for liver TICs in *MAFF*-KO and control cells. Typical images are shown in the left panel and TIC ratios are shown in the right panel. (**E**) Sphere formation of *MAFF*-KO cells. Representative sphere photos are in the left panel and sphere formation ratios are in the right panel. Each group used 5000 cells. Scale bars: 500 μm. In all panels, data are shown as mean ± SD. **P* < 0.05, ***P* < 0.01, and ****P* < 0.001 by 1-way ANOVA. For **B–E**, *n* = 3 independent experiments performed with similar results.

ure 6C). We also rescued the top 10 transcription factors whose expression levels are decreased in *cia-MAF*–KO cells, and found that only MAFF was involved in cia-MAF's function (Supplemental Figure 6D). These results indicate that cia-MAF functions mainly through MAFF.

Maff-KO liver cancer cells, which were generated using a CRISPR/Cas9 approach, were characterized by reduced expression of TIC markers and proliferation marker Ki67 (Figure 6, A–C). Moreover, impaired self-renewal and tumor initiation capacities were observed in *Maff*-KO cells (Figure 6, D and E). CD44 expression was also impaired in *Maff*-KO spheres (Figure 6F). Overall, these findings indicate that cia-MAF promotes self-renewal of human and mice liver TICs via a MAFF-dependent manner.

cia-MAF interacts with the TIP60 complex. To explore the molecular mechanisms by which cia-MAF regulates MAFF expression, we performed an RNA pulldown assay using cia-MAF, and mass spectrum analysis identified TIP60, RUVBL2, and P400 as cia-MAF partners in the tumor spheres, and their interaction was confirmed by Western blot (Figure 7, A and B).

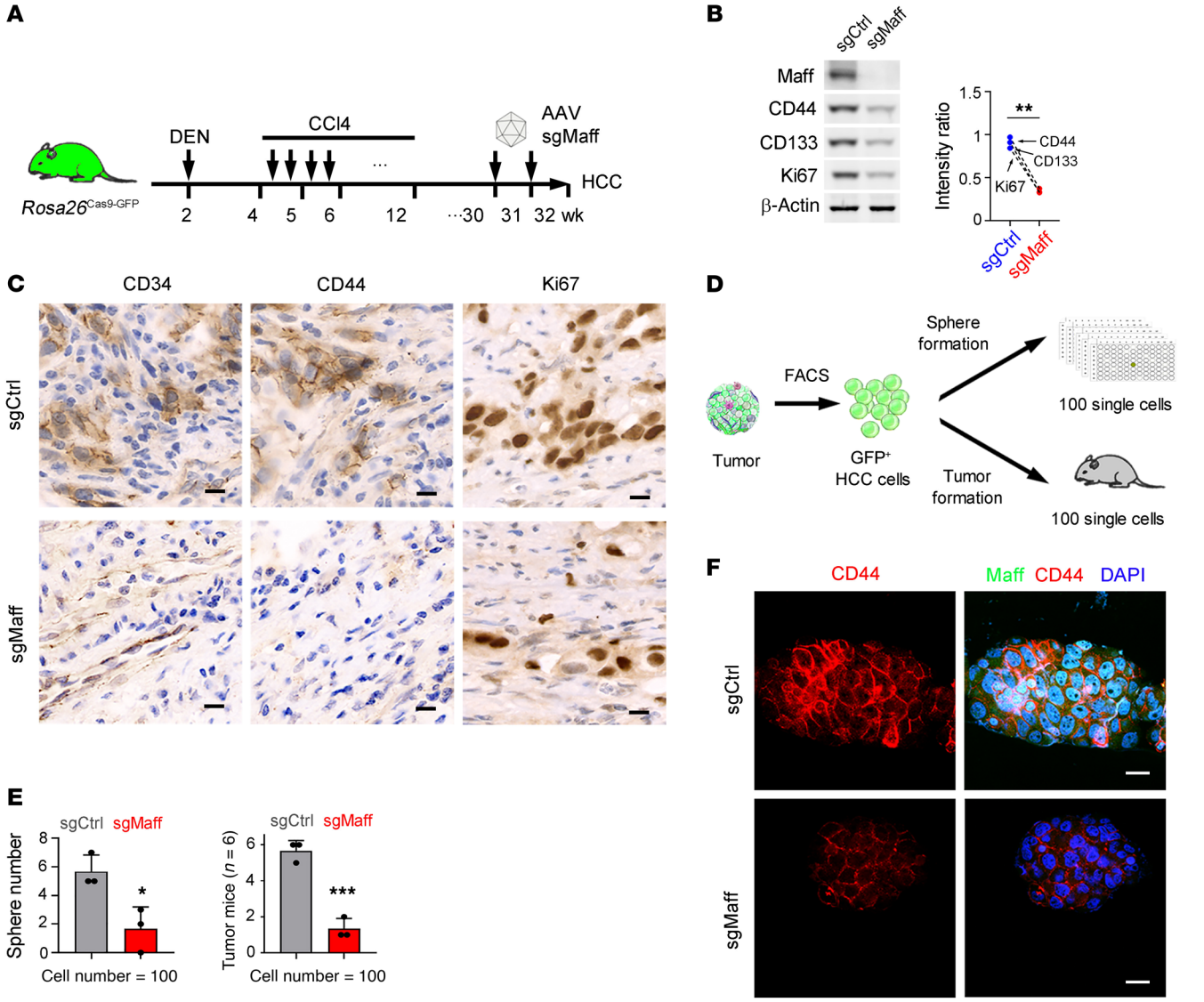

Figure 6. Maff is required for liver tumorigenesis and liver TIC self-renewal. (**A**) Schematic diagram of CRISPR/Cas9 in vivo knock out in liver cancer cells using AAV method. DEN and CCl4 were used to induce liver tumorigenesis. (**B**) Western blot to detect the expression levels of Maff and TIC markers in GFP$^+$ cells, which were isolated from sgCtrl and sgMaff liver tumors at 32 weeks. $^{**}P < 0.01$, by 1-tailed Student's *t* test. (**C**) CD34, CD44, and Ki67 immunohistochemistry in *Maff*-KO and control liver tumors. Scale bars: 20 μm. (**D**) CRISPR/Cas9-based construction of *Maff*-KO liver cancer cells, followed by sphere formation and tumor initiation. (**E**) Sphere formation (left) and tumor initiation (right) of *Maff*-KO and control cells. Each group used 100 single cells and 6 mice for tumor initiation assay. Data are shown as mean ± SD. $^{*}P < 0.05$ and $^{***}P < 0.001$ by 1-tailed Student's *t* test. (**F**) CD44 immunofluorescence in *Maff*-KO and control spheres. Scale bars: 10 μm. For all representative images, $n = 3$ independent experiments performed with similar results.

Tagged RNA affinity purification (TRAP) assay and RNA immunoprecipitation validated the combination between cia-MAF and the TIP60 complex (Figure 7C, and Supplemental Figure 7, A and B). Furthermore, split GFP assay and FISH confirmed that cia-MAF was colocalized with P400, the core component of the TIP60 complex (Figure 7, D and E, and Supplemental Figure 7C). These data demonstrate that cia-MAF interacts with the TIP60 complex.

TRAP assay using truncated cia-MAFs lacking individual exons revealed that the first exon of cia-MAF is required for the interaction between cia-MAF and P400 (Supplemental Figure 7, D and E). Considering the critical role of stem loops in the RNA interactome (30, 31), we performed loop mutation analyses and found that HR#3 was essential for the interaction between cia-MAF and P400 (Supplemental Figure 7, F and G). Moreover, the regulatory functions of truncated cia-MAF and HR#3-mutant cia-MAF in liver TIC self-renewal and invasion were impaired, suggesting that the interaction with TIP60 complex is critical for the function of cia-MAF (Figure 7F and Supplemental Figure 7H).

We also assessed the function of the TIP60 complex in liver TICs. We observed significant reductions of TIC ratio and self-renewal ability in TIP60-inhibited cells, demonstrating the essential role of TIP60 in liver TICs (Figure 7, G and H). Unlike in control cells, the effects of cia-MAF overexpression on liver TIC ratio, sphere formation, and invasion were impaired upon TIP60

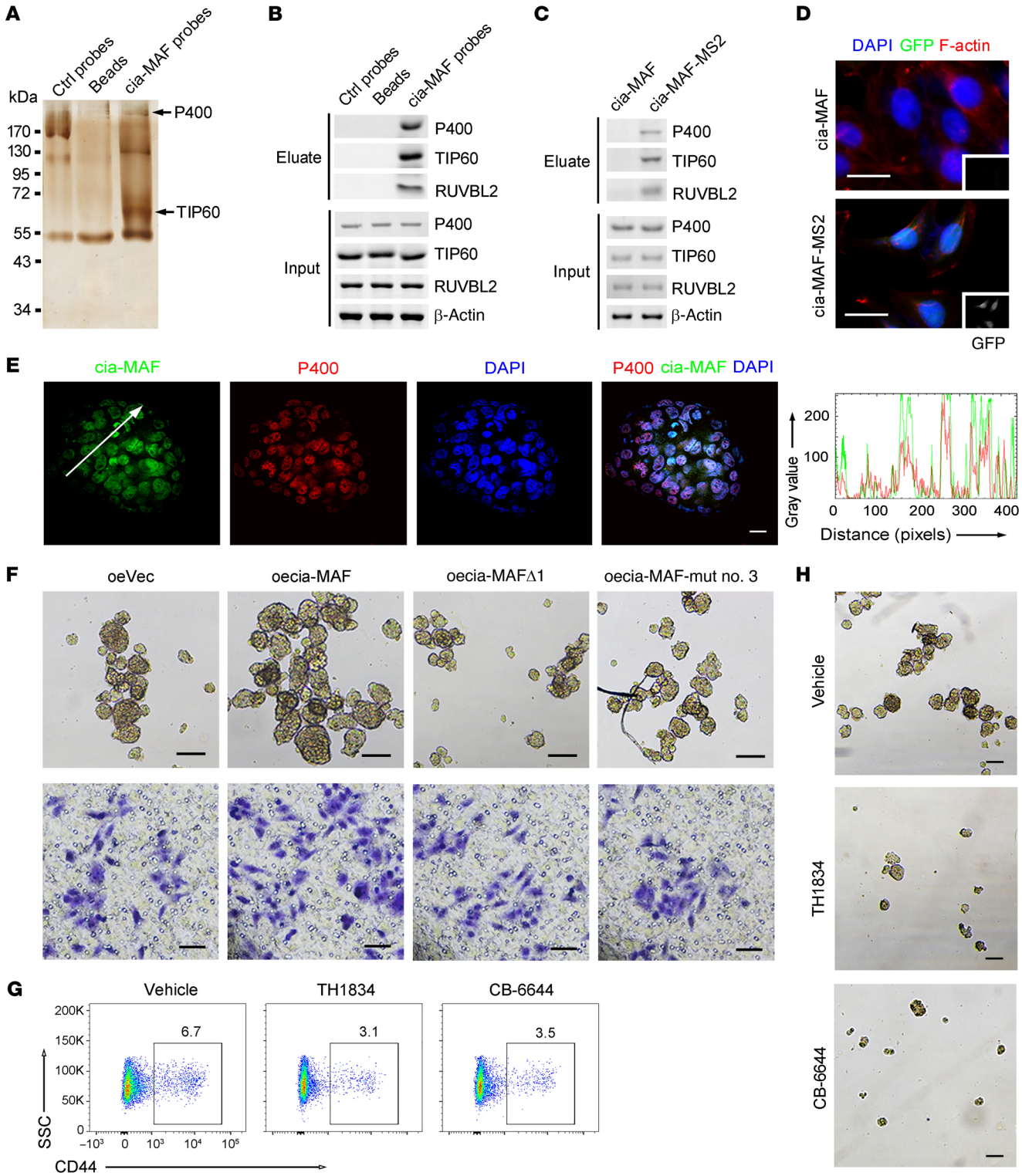

Figure 7. cia-MAF interacts with TIP60 complex. (**A**) Sliver staining of eluate sample from RNA pulldown assay, for which Biotin-labeled cia-MAF probes and sphere cell lysate were used. (**B**) Western blot for the interaction between cia-MAF and P400, TIP60, and RUVBL2. (**C**) Western blot to detect the enrichment of TIP60 complex in eluate from TRAP assay, for which cia-MAF-MS2 and MCP-GST binding system was used. (**D**) Split GFP assay to detect the combination of cia-MAF and P400. The GFP signal was shown in bottom right. Scale bars: 10 μm. (**E**) Colocalization of cia-MAF and P400 in spheres. cia-MAF and P400 were visualized by FISH and immunofluorescence, respectively. The gray values of P400 (red) and cia-MAF (green) signals along the white arrow (left) were in right. Scale bars: 10 μm. (**F**) Sphere formation (upper) and transwell (lower) assays of primary cells, in which WT cia-MAF, truncate cia-MAF, or mutant cia-MAF were overexpressed. Scale bars: 500 μm (upper panels), 70 μm (lower panels). CD44 FACS (**G**) and sphere formation (**H**) of liver cancer cells treated with TH1834 or CB-6644, 2 inhibitors of the TIP60 complex. Scale bars: 500 μm. For all representative images, *n* = 3 independent experiments performed with similar results.

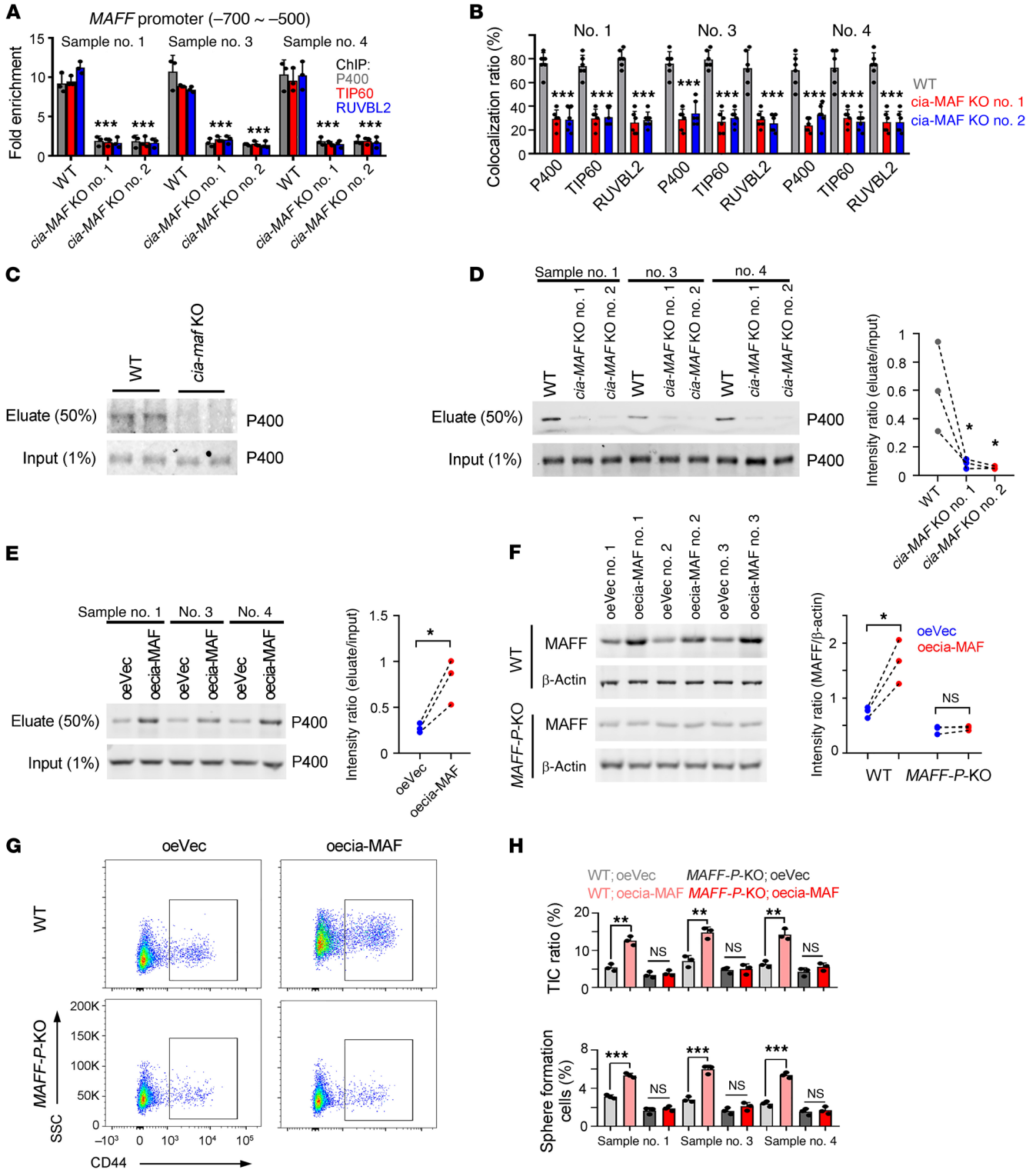

Figure 8. cia-MAF recruits the TIP60 complex to the *MAFF* promoter. (**A**) Real-time PCR to detect the enrichment of *MAFF* promoter in eluate from ChIP assay, for which P400, TIP60, and RUVBL2 antibodies and *cia-MAF*–KO spheres were used. $n = 3$ independent experiments. (**B**) Colocalization of *MAFF* promoter and TIP60 components (P400, TIP60, and RUVBL2) in *cia-MAF*–KO and control cells. $n = 6$ independent experiments. Western blot to detect P400 in eluate from CAPTURE assay, for which *cia-maf*–KO sphere (**C**) or *cia-MAF*–KO spheres (**D**) were used. For **C**, WT littermates were used as controls. (**E**) Western blot for P400 in eluate from CAPTURE assay using cia-MAF–overexpressing and control spheres. (**F**) Western blot for MAFF detection upon cia-MAF overexpression, which was performed in *MAFF* promoter knockout cells. (**G** and **H**) CD44 FACS and sphere formation upon cia-MAF overexpression, which were generated in WT and *MAFF-P*–KO cells. $n = 3$ independent experiments. In all panels, data are shown as mean ± SD. $^*P < 0.05$, $^{**}P < 0.01$, and $^{***}P < 0.001$. Significance was determined by 1-way ANOVA (**A**, **B**, and **D**) or 1-tailed Student's *t* test (**E**, **F**, and **H**). For **D**–**F**, typical images are in the left panel and signal intensities quantified with Image J are in the right panel. For all representative images, $n = 3$ independent experiments performed with similar results.

blockade, confirming the critical role of TIP60 in the function of cia-MAF (Supplemental Figure 7I). Altogether, cia-MAF interacts with the TIP60 complex to drive liver TIC self-renewal.

cia-MAF recruits TIP60 to the MAFF promoter and initiates its expression. We then analyzed the mechanisms by which cia-MAF and TIP60 regulate MAFF expression. Interestingly, TIP60 and cia-MAF bind to the same region of the *MAFF* promoter (Supplemental Figure 8A). Thus, we evaluated the potential role of cia-MAF in the interaction between the TIP60 complex and the *MAFF* promoter. The enrichment of the TIP60 complex onto the *MAFF* promoter was attenuated in *cia-MAF*–KO cells, but was enhanced upon cia-MAF overexpression (Figure 8A and Supplemental Figure 8, B and C). The requirement of cia-MAF in the association of *MAFF* promoter and TIP60 complex was confirmed by FISH (Figure 8B and Supplemental Figure 8D). CRISPR affinity purification in situ of regulatory elements (CAPTURE) assay (32) confirmed that the interaction between TIP60 complex and *MAFF* promoter was impaired in *cia-MAF*–KO cells but was enhanced in cia-MAF–overexpressing cells (Figure 8, C–E, and Supplemental Figure 8E).

Considering the critical role of the TIP60/P400 complex in histone acetylation, we examined H3K9ac, H3K14ac, and H4K12ac levels in the *MAFF* promoter, and found impaired histone acetylation in *cia-MAF*–KO cells (Supplemental Figure 8F). Moreover, the *cia-MAF*–KO cells also contained decreased levels of H3K4me3, providing further evidence that cia-MAF is required for the activation of the *MAFF* promoter (Supplemental Figure 8G). An RNA polymerase II ChIP assay also confirmed that cia-MAF activated the *MAFF* promoter (Supplemental Figure 8H). Taken together, cia-MAF activates the *MAFF* promoter via recruiting TIP60 complex.

To further validate the role of cia-MAF in *MAFF* promoter activation, we generated *MAFF* promoter (*MAFF-P*) knockout cells, which lost the cia-MAF binding region (Supplemental Figure 8I). Of note, the regulatory function of cia-MAF on MAFF expression was impaired in *MAFF*-P–KO cells (Figure 8F). Furthermore, cia-MAF overexpression had negligible effects on the liver TIC ratio, self-renewal, and invasion capacities of *MAFF*-P–KO cells (Figure 8, G and H, and Supplemental Figure 8J). These results confirm that cia-MAF functions through the *MAFF* promoter and MAFF transcription. Altogether, cia-MAF recruits the TIP60 complex to the *MAFF* promoter and drives MAFF expression.

MAFF drives liver TIC self-renewal and can be targeted in HCC samples without the MAFA/MAFG gene CAN. We next analyzed MAFF expression in HCC samples. First, online-available data demonstrated increased expression of MAFF in HCC, especially in patients with metastasis, relapse, and severe clinical features (Supplemental Figure 9A and Supplemental Table 6). MAFF expression was also related to the prognosis of patients with HCC (Supplemental Figure 9, B and C). The increased expression of MAFF in liver cancer and liver TICs was confirmed by Western blot and immunofluorescence staining (Figure 9, A and B).

We then used MAFF ASO for HCC therapy. MAFF ASO showed remarkable effects on sphere formation in some HCC samples, but not in others (Figure 9, C and D). Considering the potential roles of other MAF TFs in MAFF-inhibited cells, and the high frequency of *MAFA/MAFG* gene CNAs in HCC (33), we raised a hypothesis that the divergent functions of MAFF ASO may originate from the abnormal expression landscape of MAF TFs due to *MAFA/MAFG* gene CNAs. Thus, we analyzed the CNAs of *MAFA* and *MAFG* loci in 72 HCC samples, and detected *MAFA/MAFG* CNAs in 17 samples (Supplemental Figure 9, D and E). Interestingly, *MAFA/MAFG* gene CNAs changed the expression landscape of MAF TFs, because MAFF expression was the greatest in samples without CNAs whereas MAFG expression was the greatest in samples with CNAs (Supplemental Figure 9F). In patients with *MAFA/MAFG* gene CNAs, MAFG probably still functions via a MAFF-like manner upon MAFF-ASO treatment. To clarify this, we constructed a MAFF-reporter system with 4 times MAFF-driven GFP expression, and established MAFF reporter cells (Supplemental Figure 9G). As expected, MAFF and MAFG both promoted MAFF-driven GFP expression (Supplemental Figure 9H). We also generated a MAFF-reporter system in primary cells with or without *MAFA/MAFG* gene CNAs. In *MAFA/MAFG* non-CNA cells, MAFF ASO treatment significantly attenuated MAFF-driven GFP expression, while in *MAFA/MAFG* CNA cells, the effect of MAFF ASO was limited (Supplemental Figure 9I). These results confirmed the efficiency of MAFF ASO in *MAFA/MAFG* non-CNA cells, and indicated that the limited efficiency of MAFF ASO was partially due to MAFG, which shared the similar DNA-binding sequence with MAFF (Supplemental Figure 9J).

Indeed, the HCC cells that were responsive to the ASO treatment harbored no *MAFA/MAFG* gene CNAs, whereas all non-responsive cells harbored *MAFA/MAFG* gene CNAs, which is consistent with our hypothesis. In addition to suppressing TIC self-renewal and invasion, MAFF ASO also blocked tumor propagation, prolonged the survival time, impaired TIC maintenance, and decreased CD44 expression in the responsive cells (Figure 9, E–G). Altogether, these findings demonstrate that MAFF ASO has powerful effects on suppressing tumor propagation and TIC activity in liver cancer cells without *MAFA/MAFG* gene CNAs.

Discussion

The molecular mechanisms of liver TIC regulation are elusive, which largely limits the clinical application of TICs. Previously, we identified several modulators of liver TICs, including transcription factor Zic2, long noncoding RNA lncBRM, and lnc-β-catm (15, 34, 35). In this study, we identified cia-MAF, a robustly expressed circRNA in liver cancer and liver TICs, that regulates liver TIC maintenance and activity. We showed that cia-MAF binds to the *MAFF* promoter and recruits the TIP60 chromatin remodeling complex to initiate MAFF transcription. MAFF ASO is an effective strategy to eliminate TICs, especially for patients with HCC without *MAFA/MAFG* gene CNAs (Supplemental Figure 10). Our work has revealed an additional regulatory mechanism involved in liver TIC self-renewal and circRNA function.

It has been reported that circRNAs regulate gene expression at transcriptional and posttranscriptional stages through several mechanisms. For example, some circRNAs act as molecular sponges that bind to and block miRNAs (25, 26). Other circRNAs regulate the expression of their parental genes (36, 37) or encode peptides and exert their effects via a peptide-dependent manner (38, 39). Our recent study revealed that circPan3 was highly expressed in intestinal stem cells and blocked the Ksrp-dependent degradation of *Il13ra1* mRNA, which promoted the stability of *Il13ra1* mRNA and ultimately maintained the interaction of

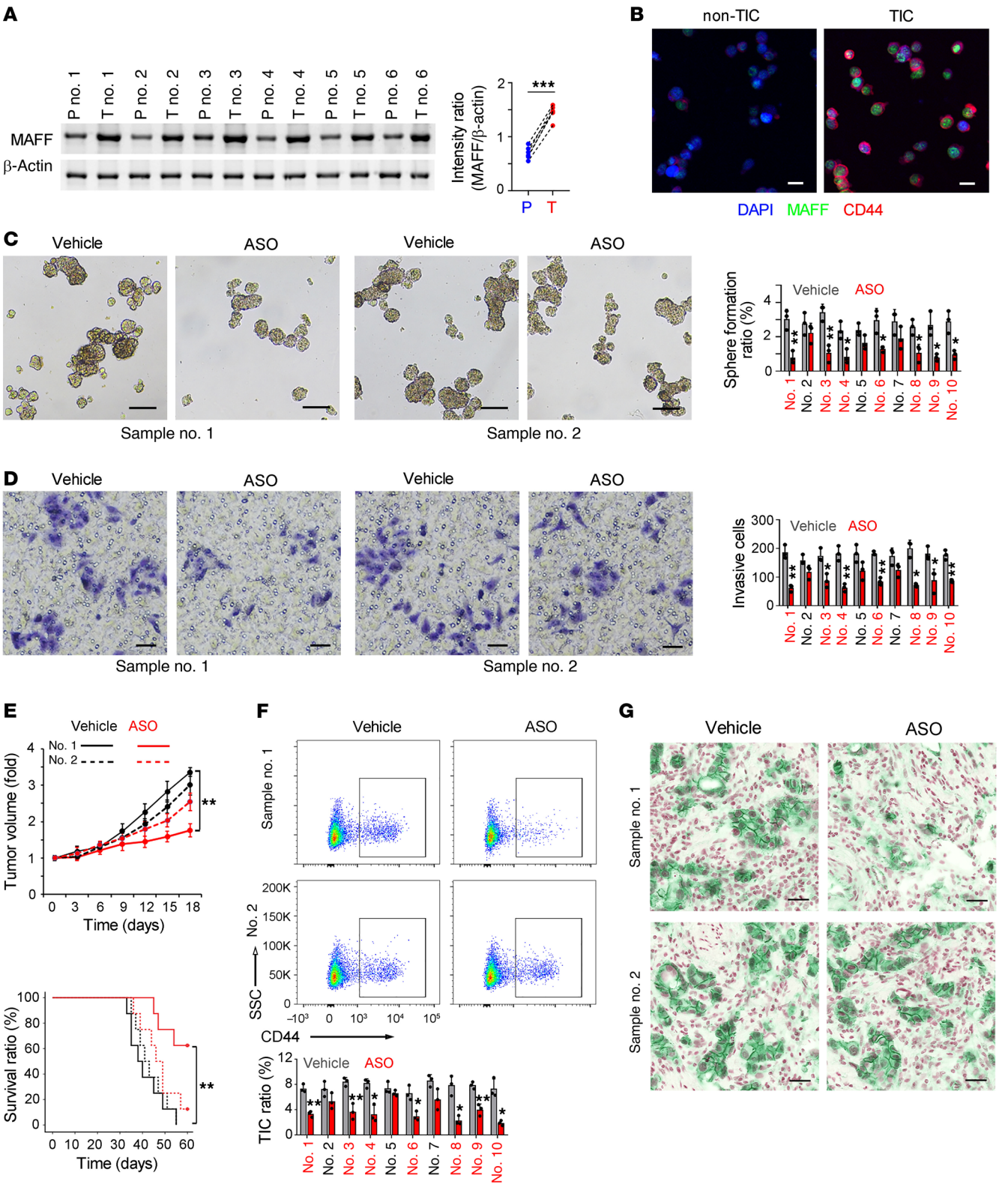

Figure 9. MAFF serves as a target for liver tumors without MAFA/MAFG CNA. (**A**) Western blot for MAFF expression in liver tumor (T) and peri-tumor (P) samples. Typical images are shown in the left panel and signal intensities are in the right panel. (**B**) Immunofluorescence of CD44 and MAFF in CD44$^+$ TICs and CD44$^-$ non-TICs. Scale bars: 10 μm. Sphere formation (**C**) and transwell (**D**) detection of HCC primary cells, which were treated with MAFF ASO 1 week before detection. MAFF ASO responders (#1, #3, #4, #6, #8, #9, and #10) are labeled red. Scale bars: 500 μm (**C**), 70 μm (**D**). (**E**) Tumor volume and survival analyses of MAFF ASO–treated primary cells. Patient-derived xenografts were treated with ASO when xenograft volume reached about 400 mm^3 (upper panel). Kaplan-Meier survival analysis of $n = 7$ mice are shown (lower panel). CD44 FACS detection (**F**) and immunohistochemistry (**G**) using MAFF ASO–treated and control xenografts. Scale bars: 50 μm. In all panels, data are shown as mean ± SD. *$P < 0.05$, **$P < 0.01$, ***$P < 0.001$. Significance was determined by 1-way ANOVA (**E**, upper panel), log-rank test (**E**, lower panel), or 1-tailed Student's t test (**A**, **C**, **D**, and **F**). For all representative images, $n = 3$ independent experiments performed with similar results.

immune cells and stem cells (29). In this study, cia-MAF modulates the activity of the *MAFF* promoter by binding to the TIP60 chromatin remodeling complex and recruiting it to the *MAFF* promoter. This mechanism indicates that circRNAs also act as molecular scaffolds to regulate gene transcription. Moreover, we confirmed that the regulatory effects of cia-MAF are conserved in mice and human samples. It is generally believed that the conservation of gene function across species indicates the gene's importance. The conserved functions of cia-MAF suggest that it plays an essential role in liver tumorigenesis and TIC function. Moreover, a transcript generally functions via a network, while cia-MAF exerts its role mainly through MAFF. cia-MAF regulates the expression of quite a few genes and transcription factors, but mainly functions through MAFF, because of the following possible reasons. First, the "true" target genes are probably not so many as they appear. Some differently expressed genes (DEGs) may not be targeted by cia-MAF itself, but by cia-MAF interacting proteins or a few "true" target genes. Second, many genes are not involved in liver TIC self-renewal and metastasis, thus they are not "functional" target genes in our TIC research. Third, some genes may function in TIC sphere-formation, but their redundant genes weaken their real functions and thus are excluded. Fourth, we screened functional target genes in primary cells, and other possible targets may exist in other liver cancer cells because of heterogeneity between different patients. Last, MAFF is only a target gene of cia-MAFF in liver TICs. cia-MAFF probably targets other genes in another physiological or pathological process, which needs to be further investigated.

Several liver TIC markers, including CD44, CD13, CD133, and EPCAM, have been identified, and some markers are also involved in the self-renewal of liver TICs. CD13 inhibition suppresses the self-renewal and tumor initiation capacities of liver TICs (40). CD133 suppression impairs the stemness properties and enhances chemoradiosensitivity of liver TICs (41). CD44 induces the nuclear-translocation of Mdm2 to terminate the genomic surveillance response by p53, and thus promotes liver tumor initiation (42). Here we found that CD44 is a target gene of MAFF in liver TICs, and cia-MAFF/MAFF functions via both CD44-dependent and CD44-independent manners.

Tumorigenesis involves reprogramming alongside chromatin remodeling. Many components of the chromatin remodeling complexes are abnormally regulated during tumorigenesis (43). We previously reported that EZH2, a core component of the PRC2 complex, is highly expressed in liver TICs and promotes Wnt/β-catenin activation and TIC self-renewal via β-catenin methylation (34). Brg1 and Brm, 2 exclusive core components of the SWI/SNF complex, undergo a BRG1-BRM switch during liver tumorigenesis (15). As an important chromatin remodeling complex, TIP60 is involved in histone acetylation, DNA repair, and regulation of apoptosis (44). However, its role in TICs remains unclear. Here, we found that TIP60 inhibitors significantly suppressed the self-renewal and metastatic capacities of liver TICs, demonstrating the important roles of TIP60 in liver TICs. Furthermore, the TIP60 complex was recruited by cia-MAF to the *MAFF* promoter, where it enhanced chromatin accessibility. Thus, our work has revealed an additional function of the TIP60 complex and an additional regulatory layer for circRNAs.

Gene knock out is widely used to study gene function, and studies using knockout mice over the last 20 years have confirmed the roles of oncogenic and tumor suppressor genes such as PTEN, P53, and ARID1A in liver tumorigenesis (45). In recent years, the number of knockout mice and knockout cells has increased rapidly due to the use of CRISPR/Cas9-based approaches (46). We previously generated *lncHand2*-KO mice, in which liver tumorigenesis and TIC self-renewal were impaired (47). In the present study, we focused on circRNAs, which are difficult to knock out. Knocking out circRNAs themselves is not feasible because of the exons of the linear parental gene. Based on the necessity of the pairing of intron complementary regions in circular RNA formation, we constructed circRNA-KO cells. We generated *cia-MAF*–KO cells by deleting the reverse complementary sequences, which were identified via minigene assay. We believe that this method will become a standard scheme for circRNA knock out, especially for circRNAs composed of exons.

Compared with normal cells, tumor cells harbor more unstable chromosomes with frequent mutations and gene CNA, 2 common chromosome aberrations detected in tumors (48, 49). CNA plays a key role in tumorigenesis and progression, and is closely related to gene expression level (50–52). Hyperactivated oncogenic genes in liver tumorigenesis, such as *c-MYC*, *FGFR*, *BCL2L1*, *DLC1*, *PRKC1*, and *SOX2*, are often copy-number gained, whereas genes with decreased expression, including *ARID1A* and *RPS6KA3*, are associated with copy number deletion (50). Here, we showed that *MAFA* and *MAFG* are frequently copy-number gained in patients with HCC, and that MAFG is highly expressed in samples with CNAs. Of note, the MAFF ASO inhibited liver TIC self-renewal and liver tumorigenesis in cells without *MAFA/MAFG* gene CNAs, but not in cells with *MAFA/MAFG* gene CNAs. MAFF and MAFG bind to similar DNA sequence, and thus MAFF ASO showed limited function in samples with MAFA/MAFG CNA, in which MAFG is highly expressed. These cellular and molecular heterogeneities greatly complicate tumor therapy, which underscores the need for precision medicine and personalized therapy. Based on the different responses to MAFF ASO treatment between *MAFA/MAFG* CNA and non-CNA HCC samples, our study provides an example of precision medicine that exploits the broad heterogeneities of liver cancer.

Conclusion. The molecular mechanisms involved in the regulation of liver TICs remain elusive. Here, we identified a circular RNA, termed cia-MAF, which is required for liver TIC self-renewal. We found that cia-MAF drives liver TIC self-renewal via its target gene MAFF. cia-MAF binds to and activates the *MAFF* promoter by recruiting the TIP60 complex to the promoter. Moreover, administration of MAFF ASO elicited antitumor effects against primary liver cancer cells lacking *MAFA/MAFG* gene CNAs. These findings suggest the cia-MAF/MAFF axis is a therapeutic target for precision medicine and personalized therapy.

Methods

Reagents and antibodies. Anti-CD133 (catalog 130-090-853) and PE-conjugated anti-CD133 antibodies were purchased from Miltenyi Biotec. PE-conjugated anti-human CD44 antibody (catalog 550989) was obtained from BD Biosciences. APC-conjugated anti-CD44 anti-

body (catalog 17-0441-81) was purchased from eBioscience. Anti-TIP60 antibody (catalog GTX112198) was purchased from GeneTex. Anti-RUVBL2 (catalog 10195-1-AP), anti-MAFF (catalog 12771-1-AP), and anti-CD44 (catalog 15675-1-AP) antibodies were obtained from Proteintech. Anti-digoxin (catalog ab51949) and anti-Ki67 (catalog ab15580) antibody was obtained from Abcam. Anti–β-actin (catalog RM2001) antibody was purchased from Beijing Ray Antibody Biotech. Alexa-594–, Alexa-488–, and Alexa-647–conjugated anti-rabbit and anti-mouse secondary antibodies were purchased from Invitrogen. HRP-conjugated secondary antibodies were purchased from Sungene Biotech. Biotin labeled RNA mix (catalog 11685597910) was obtained from Roche. Chemiluminescent nucleic acid detection module (catalog 89880) was purchased from Thermo Fisher Scientific. ChIP assay kit (catalog 17-295) was purchased from Miltenyi Biotec. Supplements N2 and B27 were purchased from Life Technologies.

CRISPR/Cas9 knock out. For *cia-maf*–KO, the essential role of intronic complementary sequences (upstream, chr5: 147443486-147443724; downstream, chr5: 147509043- 147509284) in cia-maf formation was confirmed, and the downstream complementary region was targeted by sgRNAs with the following sequences: 5′-TCTGTGTTGACAAAGAGGGC-3′ and 5′-TGGGAAAGACCCTTACACGG-3′. Approximately 250 zygotes in C57BL/6 background were injected with these 2 sgRNAs and CRISPR/Cas9, and subsequently transferred to the uterus of pseudo-pregnant ICR (Institute of Cancer Research) females, from which viable founder mice were obtained. F0 mice were genotyped by PCR primers with the following sequences: 5′- TCAATCAACATGGTTTTGTCACT-3′ and 5′-AATTAAGAGCCCTGCCTGGT-3′. All genotypes were verified by DNA sequencing. WT allele had a PCR length of about 2727 bp and deficient allele had a PCR length of about 343 bp. F0 mice were crossed to generate *cia-maf*–deficient mice. Littermate WT mice were used as controls for *cia-maf*–KO experiments, and heterozygous mice were used for *cia-maf*–KO and littermate breeding.

Knockout cells were generated through standard approach, with minor modifications (53). Generally, sgRNAs were designed and cloned into LentiCRISPRv2 (Puro, catalog 52961). LentiCRISPRv2, pVSVg (catalog 8454), and psPAX2 (catalog 12260) were used to generate CRISPR/Cas9 lentivirus, which was used to infect liver cancer cells for gene knock out. For cia-MAF–KO #1, sgRNAs 5′- CTGAAATGTTGAGTAAATCA-3′ and 5′-TGTTAAGATCAAGCTCCAAG-3′ were used for knock out, and PCR primers 5′-CAAGTGCTGGTATTTATAGA-3′ and 5′-AGTACTAAAGTTCTCAATAA-3′ were used for detection. WT allele had PCR products of about 822 bp in length and deficient allele had PCR products of about 273 bp in length. For cia-MAF–KO #2, sgRNAs 5′-TAGACTCAATTCATTAAGAG-3′ and 5′-AGTTCTGATTCATTAGGTAT-3′ were used for knock out, and PCR primers 5′-GAAGTTGTACAGTAAAGAAA-3′ and 5′- CTAAGGTGGTATTATCACTT-3′ were used for detection. WT allele had PCR products of about 723 bp in length and deficient allele had PCR products of about 291 bp in length.

Primary liver cancer cells and TIC isolation. Primary HCC cells were obtained from patients with HCC, and fresh liver cancer tissues were washed 3 times and kept in DMEM/F12 medium supplemented with 1000 U/mL penicillin and 1000 U/mL streptomycin, and transferred to the lab on ice quickly. Then the samples were washed with precooled sterile PBS containing 100 U/mL penicillin and 100 U/mL streptomycin, cut into small fragments, and digested with HBSS containing 0.03% pronase, 0.05% type IV collagenase, and 0.01% deoxyribonuclease for 30 minutes at 37°C, during which the samples were shanked every 10 minutes. Then samples were filtered through a 100 μm nylon filter and centrifuged for 2 minutes at 50*g* in 4°C, and finally, HCC primary cells were subject to precipitation.

TICs are enriched from CD44 FACS sorting or sphere formation. For TIC enrichment, liver cancer cells were stained with CD44 antibody and $CD44^+$ liver TICs were enriched by FACS. For sphere formation, 5000 primary cells were seeded into sphere formation medium and cultured in Ultra Low Attachment 6-well plates (Corning Incorporated Life Sciences, catalog 19019043).

Tumor-initiating assay. For tumor initiation assay, 10, 1×10^2, 1×10^3, 1×10^4, and 1×10^5 *cia-MAF*–KO, overexpression, and control cells were subcutaneously injected into 6-week-old BALB/c nude mice as described (54), followed by 3 months of tumor initiation, and the ratios of tumor-free mice were calculated. Seven mice were used for each sample.

Sphere formation. For sphere formation, 5000 primary cells were seeded into Ultra Low Attachment 6-well plates, and cultured in Dulbecco's modified Eagle's medium/F12 (Life Technologies) supplemented with N2, B27, 20 ng/mL EGF, and 20 ng/mL bFGF (Millipore). Sphere initiating ratio = (sphere number) /5000 × 100%.

Transwell assay. A quantity of 1×10^5 *cia-MAF*–KO, cia-MAF–overexpressing, or control cells were seeded into a top chamber with matrigel-coated membrane (Thermo Fisher Scientific) and incubated with medium without FBS, and then FBS containing medium was added into the lower chamber as a chemoattractant. After 36 hours of incubation at 37°C, cells that did not penetrate the membrane were scraped off with a cell scraper, and the cells on the lower surface of the chamber membrane were fixed with methanol and stained with crystal violet. Images were then taken with a Nikon Eclipse Ti2-U microscope.

MAFF ASO treatment. For transfection of MAFF ASO in vitro, 5×10^4 primary cells were transfected with MAFF ASO (50 nM) or control ASO with RNAiMax according to the manual. The MAFF ASO sequence was designed and synthesized by Guangzhou RiboBio Co., Ltd. For in vivo transfection, we began to perform intratumoral injections of scrambled or in vivo–optimized MAFF ASO (5 nmol per injection, RiboBio) every 3 days when xenograft volume reached about 400 mm^3. Tumor volume was also measured every 3 days.

Hydrodynamic injection. HrasG12V, shp53, luciferase, and SB transposases were hydrodynamically injected into *cia-maf*–KO and control mice (55). HrasG12V was cloned from pbabe-c-mycT58A+HRasG12V plasmid (Addgene 11130) to pT2-shP53 (Addgene 124261). A quantity of 15 μg luciferase and SB transposases expressing plasmid (Addgene 20207) and 15 μg HRasG12V-shP52 plasmid was suspended in 1.6 mL Ringer's solution and was then injected into the tail veins of 6-week-old *cia-maf*–KO and littermate mice in less than 7 seconds, and tumor formation was detected through luciferase signals.

Copy number detection by real-time PCR. Chromatin DNA was extracted from 72 clinical samples, and the content of MAFA, MAFG, ACTB, and GAPDH DNA fragments (crossing extron-intron junctions) were analyzed by real-time PCR. Relative levels of MAFA and MAFG DNA (relative to ACTB and GAPDH) were analyzed individually. The samples were divided into at least 2 groups, copy-number gained and non-gained groups. The average value of the non-gained group was normalized as 2, and copy numbers of all samples were normalized accordingly.

DNase chromatin accessibility assay. For chromatin accessibility assay, cell nuclei were isolated from spheres, *cia-MAF*–KO spheres, or control spheres, and then cell nuclei were digested with 1 U/mL DNase I for 5 minutes at 37°C. After stopping the digestion, total DNA was extracted and measured by real-time PCR.

CRISPR affinity purification in situ of regulatory elements. CAPTURE assay was performed as described (32). Briefly, pEF1a-BirA-V5-neo (Addgene 100548), pEF1a-FB-dCas9-puro (Addgene 100547), and sgRNA targeting *MAFF* promoter were overexpressed in liver cancer cells for intracellular dCas9 biotinylation. After purification with Streptavidin, enrichment of cia-MAF at *MAFF*-P locus was detected through real-time PCR. *MAFF-P*–KO and control cells were also used for CAPTURE assay, and the enrichment of cia-MAF in *MAFF* promoter was examined by real-time PCR.

Tagged RNA affinity purification. TRAP assay was performed as described (56). cia-MAF conjugated with MS2 sequence, and MS2 coat protein (MCP, cloned from Addgene 75384) conjugated with GST plasmids were overexpressed in liver cancer cells. cia-MAF binding proteins were enriched through GST pulldown assay, and detected by Western blot.

Immunohistochemistry. Immunohistochemistry assay was performed as described (57). Paraffin sections of liver cancer clinical samples, DEN/CCl4 mouse tumor tissues, and liver tumor tissue microarray were treated with xylene and gradient ethanol, and then treated by 3% H_2O_2 for 15 minutes to block endogenous peroxidase. Samples were then incubated with boiling antigen retrieval buffer for 30 minutes and incubated with CD44, CD34, Ki67, and MAFF antibodies overnight at 4°C. After staining with HRP-conjugated secondary antibodies, the samples were detected by DAB (3,3′-Diaminobenzidine tetrahydrochloride). The sections were then counterstained with hematoxylin for nuclear staining and dehydration in gradient alcohols and xylene. For CD44 and CD34 staining, citrate/sodium citrate buffer was used for antigen retrieval. For Ki67 and MAFF staining, Tris/EDTA buffer was used for antigen retrieval.

Nucleocytoplasmic separation. Spheres derived from primary HCC samples were treated with 0.5 mL resuspension buffer (10 mM HEPES, 1.5 mM $MgCl_2$, 10 mM KCl, 0.2% *N*-octylglucoside, protease inhibitor cocktail, RNase inhibitor, pH 7.9) for 10 minutes. The cytoplasmic fraction was in supernatant after homogenization and centrifugation (400*g* for15 minutes). The pellet was resuspended in 0.2 mL PBS, 0.2 mL nuclear isolation buffer (40 mM Tris-HCl, 20 mM $MgCl_2$, 4% Triton X-100, 1.28 M sucrose, pH 7.5), and 0.2 mL RNase-free H_2O, followed by 20 minutes of incubation on ice to clean out the residual cytoplasmic faction. RNA was extracted from nuclear and cytoplasmic fractions using RNA extraction kit. In our experiment, 1 mg nuclear RNA and 1 mg cytoplasmic RNA were used, with the same final volume of nuclear and cytoplasmic cDNA (50 μL). Real-time PCR was performed using 1 μL nuclear cDNA or 1 μL cytoplasmic cDNA, with the same primers and ABI QuantStudio 5. The relative cia-MAF contents were calculated with the following formulas: nuclear ratio = $2^{-Ct(nuclear)} / (2^{-Ct(nuclear)} + 2^{-Ct(cytoplasmic)})$; cytoplasmic ratio = $2^{-Ct(cytoplasmic)} / (2^{-Ct(nuclear)} + 2^{-Ct(cytoplasmic)})$. All primers for real-time PCR are listed in Supplemental Table 3.

In situ hybridization. Digoxigenin-conjugated cia-MAF probes were designed according to protocols of Biosearch Technologies (https://www.biosearchtech.com/). The tumor tissue microarray was treated sequentially by xylene, xylene, 100% ethanol, 100% ethanol, 90% ethanol, 75% ethanol, incubated in 3% H_2O_2 for 15 minutes, and then hybridized with cia-MAF probes under nondenatured conditions. All experiments were performed according to the protocol provided by Biosearch Technologies, and the sections were visualized with DAB, counterstained with hematoxylin, dehydrated, and mounted. Finally, samples were observed with a confocal microscope.

Western blot. Liver cancer cells, TICs, and spheres were lysed with RIPA buffer (50 mM Tris-HCl [pH 7.4], 150 mM NaCl, 0.5% sodium desoxycholate, 0.1% SDS, 5 mM EDTA, 2 mM PMSF, 20 mg/mL aprotinin, 20 mg/mL leupeptin, 10 mg/mL pepstatin A, 150 mM benzamidine, and 1% Nonidet P-40) for 45 minutes on ice, centrifugalized, and the supernatants were collected for protein quantification with ELISA. Samples containing 20 μg proteins were loaded to 12% SDS-PAGE for electrophoresis, and then transferred to the nitrate cellulose membrane. After incubation with probed corresponding primary antibodies and secondary antibodies, the protein levels were detected by ultra-sensitive enhanced chemiluminescent (ECL) substrate.

Chromatin immunoprecipitation. ChIP assays were performed according to the standard protocol (Upstate Biotechnology, Inc.). Spheres derived from primary or mouse liver cancer were digested with Trypsin/EDTA and treated with 1% formaldehyde for 10 minutes at 37°C, and then crushed with SDS lysis buffer for 10 minutes on ice, followed by ultrasonication to get 200–500 bp DNA fragments (Bioruptor). The supernatants containing chromatin components were used for antibody binding. The samples were precleared with salmon sperm DNA/protein agarose beads for 1 hour, and then incubated with the P400, TIP60, RUVBL2, H3K4me3, and RNA polymerase II antibodies for ChIP assay. Then enrichments were analyzed by quantitative real-time PCR, and IgG enrichment served as controls. The enrichment of *MAFF* promoter was detected by real-time PCR.

Chromatin isolation by RNA purification. For chromatin isolation by RNA purification (ChIRP) assay, spheres, *cia-MAF*–KO spheres and control spheres were cross-linked with 1% glutaraldehyde and lyzed with lysis buffer, followed by sonication to get 200–500 bp DNA fragments (Bioruptor). Biotin-labeled cia-MAF and control probes were added into cell lysates for 4 hours of incubation at 37°C with shaking, and then digoxin antibody and Protein A/G were used for the enrichment of chromatin components. The enrichment of *MAFF* promoter was detected by real-time PCR.

RNA immunoprecipitation. WT, *cia-maf*–KO, and human spheres were lyzed in RNase-free RIPA buffer (150 mM NaCl, 0.5% sodium deoxycholate, 0.1% SDS, 1% NP-40, 1 mM EDTA, and 50 mM Tris, pH 8.0, supplemented with protease-inhibitor cocktail and RNase inhibitor), and then treated with ultrasonication. Samples were centrifuged and supernatants were collected for preclear with Protein A/G. P400 antibody was incubated with Protein A/G, and then added to sphere lysates for 4 hours of incubation. Total RNA in eluate was extracted and cia-MAF enrichment was evaluated through real-time PCR. All primers for real-time PCR were listed in Supplemental Table 3.

Data viability. circRNA sequencing data of liver tumors and nontumors were deposited in the Gene Expression Omnibus (GEO) under accession code GSE78520.

Statistics. Statistical analysis of the results was performed with Microsoft Excel 2010 and statistical graphing was done with GraphPad Prism, version 8.01 (GraphPad Software), using a 1-tailed Student's *t* test for comparison between 2 groups and 1-way ANOVA with Tukey's post hoc test for comparison between multiple groups. All data represent the mean ± SEM; *P* values of less than 0.05 were considered a significant difference between groups. $^*P < 0.05$; $^{**}P <$

0.01; ***$P < 0.001$. The statistical methods and details relevant to each experiment are described in the figure legends.

Study approval. All mice were housed in the animal facility at School of Life Sciences, Zhengzhou University. This study was approved by the ethics committee of Zhengzhou University (ZZUIRB2020-54 and ZZUIRB2020-55).

Author contributions

ZC designed and performed TIC experiments, analyzed data, and wrote the paper. TL performed RNA experiments and helped with mouse genotyping and harvesting. LH and ZF provided HCC samples and analyzed data. ZW, ZY, YG, and WH performed experiments and analyzed data. PZ initiated the study, designed experiments, analyzed data, and wrote the paper. ZC, TL, ZF, and PZ edited the manuscript.

Acknowledgments

This work was supported by the Ministry of Science and Technology of China (2020YFA0803501), National Natural Science Foundation of China (31922024, 81872411, 31771638, 81921003, 31930036, and 92042302), Program for Innovative Talents of Science and Technology in Henan Province (18HASTIT042), Young Talent Support Project from Chinese Association of Science and Technology (YESS20170042), Science Foundation for Excellent Young Scholars in Henan (202300410358), and Young Talent Support Project from Henan province (2018HYTP002). We thank Zhengzhou University for supporting grants to PZ, and Modern Analysis and Computer Center of Zhengzhou University for technical support. We also thank Stallard Scientific Editing Company for their proofreading our manuscript.

Address correspondence to: Zhenzhen Chen, 100 Kexue Road, Gaoxin District, Zhengzhou 450001, Henan Province, China. Phone: 86.15838370103; Email: chenzz2015@zzu.edu.cn. Or to: Zusen Fan, 15 Datun Road, Chaoyang District, Beijing 100101, China. Phone: 86.13718706999; Email: fanz@moon.ibp.ac.cn. Or to: Pingping Zhu, 100 Kexue Road, Gaoxin District, Zhengzhou 450001, Henan Province, China. Phone: 86.18800184573; Email: zhup@zzu.edu.cn.

1. Bray F, et al. Global cancer statistics 2018: GLOBOCAN estimates of incidence and mortality worldwide for 36 cancers in 185 countries. *CA Cancer J Clin*. 2018;68(6):394–424.
2. Losic B, et al. Intratumoral heterogeneity and clonal evolution in liver cancer. *Nat Commun*. 2020;11(1):291.
3. Nio K, et al. The evolving concept of liver cancer stem cells. *Mol Cancer*. 2017;16(1):4.
4. Miao Y, et al. Adaptive immune resistance emerges from tumor-initiating stem cells. *Cell*. 2019;177(5):1172–1186.
5. Perry JM, et al. Overcoming Wnt-β-catenin dependent anticancer therapy resistance in leukaemia stem cells. *Nat Cell Biol*. 2020;22(6):689–700.
6. Zhu PP, Fan ZS. Cancer stem cell niches and targeted interventions. *Prog Biochem Biophys*. 2017;44(8):697–708.
7. Zheng H, et al. Single-cell analysis reveals cancer stem cell heterogeneity in hepatocellular carcinoma. *Hepatology*. 2018;68(1):127–140.
8. Kieckhaefer JE, et al. Liver cancer gene discovery using gene targeting, sleeping beauty, and CRISPR/Cas9. *Semin Liver Dis*. 2019;39(2):261–274.
9. Takebe N, et al. Targeting Notch, Hedgehog, and Wnt pathways in cancer stem cells: clinical update. *Nat Rev Clin Oncol*. 2015;12(8):445–464.
10. Poli V, et al. Tumorigenic cell reprogramming and cancer plasticity: interplay between signaling, microenvironment, and epigenetics. *Stem Cells Int*. 2018;2018:4598195.
11. Cheng Z, et al. Characteristics of liver cancer stem cells and clinical correlations. *Cancer Lett*. 2016;379(2):230–238.
12. Wang X, et al. Long non-coding RNA DILC regulates liver cancer stem cells via IL-6/STAT3 axis. *J Hepatol*. 2016;64(6):1283–1294.
13. Gasmi I, et al. Interleukin-17 mediates liver progenitor cell transformation into cancer stem cells through downregulation of mir-122. Paper presented at: 2018 Beijing Liver Cancer International Conference; November 2–4, 2018; Beijing, China. http://www.cancerbiomed.org/index.php/cocr/issue/view/90. Accessed August 16, 2021.
14. Chen ZZ, et al. LncFZD6 initiates Wnt/β-catenin and liver TIC self-renewal through BRG1-mediated FZD6 transcriptional activation. *Oncogene*. 2018;37(23):3098–3112.
15. Zhu PP, et al. LncBRM initiates YAP1 signalling activation to drive self-renewal of liver cancer stem cells. *Nat Commun*. 2016;7:13608.
16. Wu JY, et al. The long non-coding RNA LncHDAC2 drives the self-renewal of liver cancer stem cells via activation of Hedgehog signaling. *J Hepatol*. 2019;70(5):918–929.
17. Blank V, Andrews NC. The Maf transcription factors: regulators of differentiation. *Trends Biochem Sci*. 1997;22(11):437–441.
18. Chen YY, et al. MAFB promotes cancer stemness and tumorigenesis in osteosarcoma through a Sox9-mediated positive feedback loop. *Cancer Res*. 2020;80(12):2472–2483.
19. Moon EJ, et al. Abstract 1628: MAFF, a new hypoxia target gene involving tumor invasion and metastasis. Paper presented at: AACR 107th Annual Meeting 2016; April 16–20, 2016; New Orleans, Louisiana, USA. https://cancerres.aacrjournals.org/content/76/14_Supplement/1628.short. Accessed August 16, 2021.
20. Li X, et al. The biogenesis, functions, and challenges of circular RNAs. *Mol Cell*. 2018;71(3):428–442.
21. Zhang XO, et al. Complementary sequence-mediated exon circularization. *Cell*. 2014;159(1):134–147.
22. Piwecka M, et al. Loss of a mammalian circular RNA locus causes miRNA deregulation and affects brain function. *Science*. 2017;357(6357):eaam8526.
23. Xie R, et al. The role of circular RNAs in immune-related diseases. *Front Immunol*. 2020;11:545.
24. Van Der Steen N, et al. The circular RNA landscape of non-small cell lung cancer cells. *Cancers (Basel)*. 2020;12(5):1091.
25. Hansen TB, et al. Natural RNA circles function as efficient microRNA sponges. *Nature*. 2013;495(7441):384–388.
26. Memczak S, et al. Circular RNAs are a large class of animal RNAs with regulatory potency. *Nature*. 2013;495(7441):333–338.
27. Guarnerio J, et al. Oncogenic role of fusion-circRNAs derived from cancer-associated chromosomal translocations. *Cell*. 2016;166(4):289–302.
28. Liu B, et al. An inducible circular RNA circKcnt2 inhibits ILC3 activation to facilitate colitis resolution. *Nat Commun*. 2020;11(1):4076.
29. Zhu P, et al. IL-13 secreted by ILC2s promotes the self-renewal of intestinal stem cells through circular RNA circPan3. *Nat Immunol*. 2019;20(2):183–194.
30. Zhu P, et al. LncGata6 maintains stemness of intestinal stem cells and promotes intestinal tumorigenesis. *Nat Cell Biol*. 2018;20(10):1134–1144.
31. Liu B, et al. A cytoplasmic NF-κB interacting long noncoding RNA blocks IκB phosphorylation and suppresses breast cancer metastasis. *Cancer Cell*. 2015;27(3):370–381.
32. Liu X, et al. In situ capture of chromatin interactions by biotinylated dCas9. *Cell*. 2017;170(5):1028–1043.
33. Liu SP, et al. Identification of portal vein tumor thrombus with an independent clonal origin in hepatocellular carcinoma via multi-omics data analysis. *Cancer Biol Med*. 2019;16(1):147–170.
34. Zhu P, et al. lnc-β-Catm elicits EZH2-dependent β-catenin stabilization and sustains liver CSC self-renewal. *Nat Struct Mol Biol*. 2016;23(7):631–639.
35. Zhu P, et al. ZIC2-dependent OCT4 activation drives self-renewal of human liver cancer stem cells. *J Clin Invest*. 2015;125(10):3795–3808.
36. Zhang Y, et al. Circular intronic long noncoding RNAs. *Mol Cell*. 2013;51(6):792–806.
37. Li ZY, et al. Exon-intron circular RNAs regulate transcription in the nucleus. *Nat Struct Mol Biol*. 2015;22(3):256–264.

38. Pamudurti NR, et al. Translation of CircRNAs. *Mol Cell*. 2017;66(1):9–21.
39. Legnini I, et al. Circ-ZNF609 is a circular RNA that can be translated and functions in myogenesis. *Mol Cell*. 2017;66(1):22–37.
40. Haraguchi N, et al. CD13 is a therapeutic target in human liver cancer stem cells. *J Clin Invest*. 2010;120(9):3326–3339.
41. Lan X, et al. CD133 silencing inhibits sternness properties and enhances chemoradiosensitivity in CD133-positive liver cancer stern cells. *Int J Mol Med*. 2013;31(2):315–324.
42. Dhar D, et al. Liver cancer initiation requires p53 inhibition by CD44-enhanced growth factor signaling. *Cancer Cell*. 2018;33(6):1061–1077.
43. Wang GG, et al. Chromatin remodeling and cancer, Part II: ATP-dependent chromatin remodeling. *Trends Mol Med*. 2007;13(9):373–380.
44. Ikura T, et al. Involvement of the TIP60 histone acetylase complex in DNA repair and apoptosis. *Cell*. 2000;102(4):463–473.
45. Di Cristofano A, et al. Pten is essential for embryonic development and tumour suppression. *Nat Genet*. 1998;19(4):348–355.
46. Zuo E, et al. One-step generation of complete gene knockout mice and monkeys by CRISPR/Cas9-mediated gene editing with multiple sgRNAs. *Cell Res*. 2017;27(7):933–945.
47. Wang Y, et al. LncRNA HAND2-AS1 promotes liver cancer stem cell self-renewal via BMP signaling. *EMBO J*. 2019;38(17):e101110.
48. Lengauer C, et al. Genetic instabilities in human cancers. *Nature*. 1998;396(6712):643–649.
49. Vogelstein B, et al. Cancer genome landscapes. *Science*. 2013;339(6127):1546–1558.
50. Justilien V, et al. The PRKCI and SOX2 oncogenes are coamplified and cooperate to activate Hedgehog signaling in lung squamous cell carcinoma. *Cancer Cell*. 2014;25(2):139–151.
51. Tseng YY, et al. PVT1 dependence in cancer with MYC copy-number increase. *Nature*. 2014;512(7512):82–86.
52. Wong N, et al. Hypomethylation of chromosome 1 heterochromatin DNA correlates with q-arm copy gain in human hepatocellular carcinoma. *Am J Pathol*. 2001;159(2):465–471.
53. Chen ZZ, et al. LncSox4 promotes the self-renewal of liver tumour-initiating cells through Stat3-mediated Sox4 expression. *Nat Commun*. 2016;7:12598.
54. Chen Z, et al. LncTIC1 interacts with β-catenin to drive liver TIC self-renewal and liver tumorigenesis. *Cancer Lett*. 2018;430:88–96.
55. Ju HL, et al. Investigation of oncogenic cooperation in simple liver-specific transgenic mouse models using noninvasive in vivo imaging. *PLoS One*. 2013;8(3):e59869.
56. Yoon JH, Gorospe M. Identification of mRNA-interacting factors by MS2-TRAP (MS2-tagged RNA affinity purification). *Methods Mol Biol*. 2016;1421:15–22.
57. Chen Z, et al. The long noncoding RNA lncZic2 drives the self-renewal of liver tumor-initiating cells via the protein kinase C substrates MARCKS and MARCKSL1. *J Biol Chem*. 2018;293(21):7982–7992.